Biochimica et Biophysica Acta 1838 (2014) 2087–2098

Contents lists available at ScienceDirect

Biochimica et Biophysica Acta

journal homepage: www.elsevier.com/locate/bbamem

A proapoptotic peptide conjugated to penetratin selectively inhibits tumor cell growth

Isabel D. Alves [a], Manon Carré [b], Marie-Pierre Montero [b], Sabine Castano [a], Sophie Lecomte [a], Rodrigue Marquant [c], Pascaline Lecorché [c], Fabienne Burlina [c], Christophe Schatz [d], Sandrine Sagan [c], Gérard Chassaing [c], Diane Braguer [b,e], Solange Lavielle [c,*]

[a] Chimie et Biologie des Membranes et Nanoobjets, CBMN CNRS UMR 5248, Université Bordeaux 1, Allée Geoffroy de Saint Hilaire, 33600 Pessac, France
[b] Aix-Marseille Université, INSERM, CRO2 UMR S 911, Centre de Recherche en Oncologie Biologique et Oncopharmacologie, 27, Boulevard Jean Moulin, 13005 Marseille, France
[c] Sorbonne Universités, UPMC Univ Paris 6, Laboratoire des BioMolécules, 4 place Jussieu, CNRS UMR 7203 and ENS, LBM, Dpt de Chimie, 24, Rue Lhomond, 75005 Paris
[d] Laboratoire de Chimie des Polymères Organiques, LCPO CNRS UMR 5629, 16 avenue Pey-Berland, 33600 Pessac, France
[e] APHM, Hôpital Timone, 13005 Marseille

ARTICLE INFO

Article history:
Received 10 February 2014
Received in revised form 18 April 2014
Accepted 24 April 2014
Available online 2 May 2014

Keywords:
Cell penetrating peptide
Apoptotic peptide
Tumor cell growth inhibition
Mitochondria disruption
Peptide lipid interaction
Lipid model systems

ABSTRACT

The peptide KLA (acetyl-$(KLAKLAK)_2$-NH_2), which is rather non toxic for eukaryotic cell lines, becomes active when coupled to the cell penetrating peptide, penetratin (Pen), by a disulfide bridge. Remarkably, the conjugate KLA–Pen is cytotoxic, at low micromolar concentrations, against a panel of seven human tumor cell lines of various tissue origins, including cells resistant to conventional chemotherapy agents but not to normal human cell lines. Live microscopy on cells possessing fluorescent labeled mitochondria shows that in tumor cells, KLA–Pen had a strong impact on mitochondria tubular organization instantly resulting in their aggregation, while the unconjugated KLA and pen peptides had no effect. But, mitochondria in various normal cells were not affected by KLA–Pen. The interaction with membrane models of KLA–Pen, KLA and penetratin were studied using dynamic light scattering, calorimetry, plasmon resonance, circular dichroism and ATR-FTIR to unveil the mode of action of the conjugate. To understand the selectivity of the conjugate towards tumor cell lines and its action on mitochondria, lipid model systems composed of zwitterionic lipids were used as mimics of normal cell membranes and anionic lipids as mimics of tumor cell and mitochondria membrane. A very distinct mode of interaction with the two model systems was observed. KLA–Pen may exert its deleterious and selective action on cancer cells by the formation of pores with an oblique membrane orientation and establishment of important hydrophobic interactions. These results suggest that KLA–Pen could be a lead compound for the design of cancer therapeutics.

1. Introduction

Since their discovery about 25 years ago, the amount of publications on cell penetrating peptides (CPPs) has burst. These small peptides with their broad cell penetrating ability and lack of toxicity have been used to deliver a large variety of cargos into cells, ranging from small peptides and proteins to nucleic acids and nanoparticles [1]. One of the first discovered CPPs is penetratin, which corresponds to the third helix of the Antennapedia homeoprotein, [2] has been the object of numerous studies both in terms of applications and studies regarding its mechanism of action [to cite a few examples] [3]. Yet, one of the unsolved issues in the area of CPPs, that hampers its application in therapeutics, relates to the lack of selectivity in the targeted tissues, cells or intracellular compartments. Herein, we have coupled penetratin to a proapoptotic peptide named KLA (acetyl-$(KLAKLAK)_2$-NH_2). KLA an amphipathic peptide was first reported as antimicrobial against several bacterial strains while being non-toxic to eukaryotic cells [4]. The prokaryotic cytoplasmic membrane and eukaryotic mitochondrial membranes share common properties such as the large transmembrane potential and high content of anionic phospholipids. Based on these facts, KLA peptide, once in the cell, was then demonstrated to influence mitochondrial membrane integrity and to trigger the apoptotic program cell death [5]. In the oncology research field, mitochondria are related to both cancer cell expansion and chemotherapy-induced apoptosis. In the recent years, there is an increasing interest in designing new compounds targeting mitochondria and multiple review articles in this area have been published [6].

The coupling of KLA to a tumor blood vessel homing motif showed anticancer activity in mice [7]. KLA pro-apoptotic properties both *in vivo* and *in vitro* were later re-confirmed with a KLA–CPP conjugate, *i.e.* KLA-Arg_7 (Arg7 being a polyarginine composed of 7 arginine residues) [8]. The potential use of this conjugate as an antitumor agent when conjugated with the appropriate systemic delivery system and targeting

* Corresponding author. Tel.: +33 14432 2443.
E-mail address: solange.lavielle@upmc.fr (S. Lavielle).

http://dx.doi.org/10.1016/j.bbamem.2014.04.025
0005-2736/

moieties was proposed. In another application, malignant hematopoietic cells were killed by apoptosis by antibody-targeted delivery of KLA peptide [9]. More recently, a mixture of the amidated CPP named MPG with KLA, as well as the conjugation of KLA to a cancer-cell binding peptide (LTVSPWY) selected from peptide libraries or to a gastrin-releasing peptide (GNHWAVGHLM) were identified as apoptosis inducers in human breast adenocarcinoma cells [10].

Herein, KLA and penetratin were linked through a disulfide bond between two additional Cys residues placed in KLA *N*-terminus and penetratin *N*-terminus. Once inside the cell, the reducing intracellular milieu should allow the release of KLA as an often employed strategy [11]. We have investigated the cytotoxic properties of both the conjugate KLA–Pen and the isolated peptides KLA and penetratin. We showed that the conjugate is cytotoxic against a panel of seven human tumor cell lines of various tissue origins, including cells resistant to some conventional chemotherapy agents. The peptides alone were non toxic. No toxicity was detected in any of the three non-cancer human cell lines tested at the same concentrations. We demonstrated that KLA–Pen had a strong impact on mitochondria tubular organization instantly resulting in aggregation, selectively in cancer cells. In an attempt to understand the selectivity of the conjugate towards tumoral cells, we have looked into differences between the cellular membrane lipid composition of non-tumor and tumor cells. The eukaryotic plasma membrane is mainly composed of zwitterionic lipids (80–90%) and the small amount of anionic lipids is mainly present (4 fold more) in the inner leaflet. Studies have shown that certain tumor cells possess increased levels of phosphatidylserine in the outer leaflet; they can contain up to 8 fold more PS in their outer leaflet than healthy cells [12]. Additionally, they overexpress certain proteoglycans (anionic in nature) like syndecans and glypicans [13], which endow tumor cells with an enhanced anionic character. These differences could explain differences in terms of binding of the conjugate to the cell membrane and internalization inside cells by endocytosis or direct translocation through the plasma membrane. As a consequence, we have focused our study on the differences in terms of the lipid composition between the two types of cells. Nevertheless, it must be stressed that the differences in terms of the proteoglycan composition and other proteins could also be implicated in the selectivity of the conjugate for tumor cells, notably towards the use of distinct endocytotic pathways. Herein lipid model systems composed of pure zwitterionic lipids were used as mimics of non-cancer cell membranes and pure anionic lipids as mimics of tumor cells. It is certain that these lipid membrane composition are far from those of cells, herein we use these as general and simple models in order to get clear cut responses regarding the role of electrostatics in peptide interaction with tumor cells. Additionally, in view of the high content of anionic lipids in mitochondria (~30% anionic lipids like cardiolipin and phosphatidylinositol) the anionic lipid model is also representative of mitochondrial membranes. Results obtained with DLS, calorimetry, plasmon resonance, CD and ATR-FTIR spectroscopy show a very distinct mode of interaction of KLA–Pen with the two lipid model systems with enhanced membrane interaction and perturbation with anionic membranes. A mechanism of action is proposed based on these data, explaining the selectivity towards tumor cells of the conjugate and the action of KLA on the mitochondrial membranes.

2. Materials and methods

2.1. Materials

Dimyristoyl phosphatidylcholine (DMPC), dimyristoyl phosphatidylglycerol (DMPG), distearoyl phosphatidylcholine (DSPC) and distearoyl phosphatidylglycerol (DSPG) were purchased from Genzyme (Switzerland) and were used without further purification. Egg PC, dioleoyl phosphatidylcholine (DOPC) and dioleoyl phosphatidylglycerol (DOPG) were purchased from Avanti Lipids (Alabama, USA). The acetyl-CRQIKIWFQNRRMKWKK-NH_2 peptide was purchased from Neo-Peptide (Cambridge, UK).

2.2. Peptide synthesis

The peptides acetyl-C(Npys)-$(KLAKLAK)_2$-NH_2, acetyl-$(KLAKLAK)_2$-NH_2 and acetyl-RQIKIWFQNRRMKWKK-NH_2 were synthesized by solid phase using the Boc strategy with DCC/HOBt activation (except for Boc-Cys(NPys)-OH which was activated with DCC only). The KLA–Pen disulfide conjugate was synthesized by dissolving acetyl-CRQIKIWFQNRRMKWKK-NH_2 with 1.2 eq of acetyl-C(Npys)-$(KLAKLAK)_2$-NH_2 in a minimum volume of sodium acetate buffer (50 mM) pH 4.5. The reaction mixture was left overnight at room temperature and the conjugate was purified by RP-HPLC on a semi-preparative C8 column using a linear acetonitrile (0.1% TFA) gradient in an aqueous solution (0.1% TFA) and characterized by MALDI-TOF MS.

2.3. Human cell lines

The non-small cell lung cancer cell line (A549) and the neuroblastoma cell line (SK-N-SH) were maintained in RPMI-1640 medium (PAA). For the resistant EpoB40 and EpoB480 cells (kindly given by SB Horwitz), which derived from A549 cells, 40 nM and 120 nM Epothilone B was added, respectively. The colon cancer cell line (SW480), the glioblastoma cell line (U251), the embryonic kidney cells (HEK-293 t) and the keratinocytes (HaCaT) were maintained in DMEM medium (PAA). The other glioblastoma cell line (U87) was maintained in MEM medium (PAA). All these culture media were supplemented with 10% Fetal Calf Serum (FCS), 2 mM L-glutamine and 1% penicillin/streptomycin (Invitrogen). HEK-293 t also received 1% non-essential amino acids. The umbilical vein endothelial cells (HUVECs) were grown in standard culture RPMI 1640 containing 20% heat-inactivated FCS, 2 mM glutamine, 1% penicillin/streptomycin, 50 IU/mL sodium heparin (Sanofi–Synthelabo), and 50 Ag/mL endothelial cell growth supplement (BD Biosciences). Cell lines were routinely maintained in culture at 37 °C and 5% CO_2 and regularly screened to ensure the absence of mycoplasma contamination (MycoAlert, Lonza).

2.4. Cytotoxicity assay

Growth inhibition was measured using the 3-[4,5-dimethylthiazol-2-yl]-2,5-diphenyltetrazolium bromide (MTT) cell proliferation assay. This colorimetric assay allows the monitoring of cell survival *in vitro*. For all cell lines, the number of cells seeded (7500 per well for HEK, U87, U251, A549, EpoB40 and Epo480 cells; 15,000 per well for HUVECs, HaCaT, SW480 and SK-N-SH cells) in 96-well plates was first optimized to ensure sustained exponential growth for 4 to 6 days. Cells were treated 24 h after seeding with Pen, KLA, KLA–Pen conjugate, or an extemporaneously mixture of the two peptides for 2, 6 and 24 h. After incubation with peptides, metabolic activity was detected by addition of MTT followed by spectrophotometric analysis (550 nm). Cell proliferation was determined and expressed as a percentage of control (vehicle-treated) cells. The cytotoxicity assay was also used to determine the effects of a 24 h treatment followed by a 24 h wash-out period (*i.e.* drug-free medium) on cell viability.

2.5. Live fluorescent microscopy of the mitochondrial network

Fluorescence labeling of mitochondria was performed by transfecting SK-N-SH, U251 and A549 cells with the mitochondrion-targeted DsRed (mtDsRed) plasmid (ClonTech). Transfections were achieved using Lipofectamine 2000 (Invitrogen) according to the protocol supplied by the manufacturer. Stable transfectants were obtained after geneticin selection (800 μg/mL) for three weeks. A good fluorescence quality was ensured by cell sorting (FACScan, Becton Dickinson). In SW480, U87, HUVEC, HEK, and HaCaT cells, fluorescent mitochondria were obtained

by incubating cells with 25 mg/mL MitoTracker Red CMXRos (Molecular Probes) at 37 °C for 20 min. Living cells were then examined using a Leica DM-IRBE microscope coupled to a digital camera driven by MetaMorph software (Princeton Instruments).

2.6. Preparation of MLVs, LUVs and SUVs

Lipid films were made by dissolving the appropriate amounts of lipid in chloroform and methanol, 2/1 (v/v), followed by solvent evaporation under nitrogen to deposit the lipid as a film on the wall of a test tube. Final traces of solvent were removed in a vacuum chamber attached to a liquid nitrogen trap for 3–4 h. Films were hydrated with 10 mM Tris, 0.1 M NaCl, 2 mM EDTA, pH 7.6 (Tris buffer) (for differential scanning calorimetry DSC, isothermal titration calorimetry ITC, plasmon-waveguide resonance PWR experiments) or with 10 mM phosphate buffer, pH 7.6 (for CD, Turbidity and DLS experiments) and vortexed extensively above the melting temperature (Tm) to obtain multilamellar vesicles (MLVs). To form large unilamellar vesicles (LUVs), the MLVs were subjected to five freeze/thawing cycles. For low concentration of lipids (~1 mg/mL), the homogeneous lipid suspension was passed 19 times through a mini-extruder (Avanti Alabaster, AL) equipped with two stacked 100 nm polycarbonate membranes at a temperature above the phase transition temperature of the lipid. For higher concentrations of lipids (~10 mg/mL), the homogeneous lipid suspension was passed 10 times through a nitrogen pressure driven extruder (LIPEX, Northern Lipids Inc., BC) equipped with a 100 nm polycarbonate membrane above Tm. Small unilamellar vesicles (SUVs) were obtained by MLV sonification using a titanium rod sonifier in an ice-water bath to avoid lipid thermal degradation. Titanium traces were removed by centrifugation (6000 rpm, 2 min). In all experiments performed the peptides were added to the lipid model systems after their formation.

2.7. Measurements of liposome turbidity

Changes in aggregation state of vesicles were monitored by absorbance measurements at 436 nm. Aliquots of peptide stock solutions were added to 250 μL suspensions of LUV (lipid concentration, 1250 μM) in 10 mM sodium phosphate buffer. The absorbance was measured using a Jobin-Yvon CD6-SPEX before and after addition of peptide. The measurements were carried out at 25 and 65 °C.

2.8. Dynamic light scattering

The size distribution of liposomes following peptide addition was monitored by DLS for both DSPC and DSPG at 25 and 60 °C and for a peptide/lipid (P/L) ratio of 1/100. Due to peptide precipitation that occurred at higher peptide concentrations higher P/L ratio was not measured. Measurements were performed on a Malvern ZetaSizer Nano ZS instrument with a detection angle at 173°. Mean hydrodynamic diameters were determined by fitting the normalized time auto-correlation function of the electric field of the scattered light with the cumulant method and applying the Stokes–Einstein equation.

2.9. Calcein leakage

Calcein-containing LUVs were made using the same protocol used to make regular LUVs, except for the hydration step that was performed in presence of 70 mM calcein. Free calcein was separated from the calcein-containing LUVs using size exclusion column chromatography (Sephadex G-75) with Tris as elution buffer. The concentration of lipids was estimated using the Rouser protocol [14]. For the assay, the lipid concentration was set at 1 μM and peptide concentration was allowed to vary to allow P/L ratios of 1/100, 1/50 and 1/25. All measurements were performed with a Perkin Elmer LS55 spectrometer (Buckinghamshire, UK). Data were collected every one second at room temperature using a λ_{exc} at 485 nm and λ_{em} at 515 nm with an emission and excitation slit of 2.5 nm in a 2 mL cuvette.

The fluorescence from calcein at 70 mM concentration was low due to self-quenching, but increased considerably upon dilution. The fluorescence intensity at the equilibrium was measured after 2.5 h. At the end of the assay, complete leakage of LUVs was provoked by adding 100 μL of 10% Triton X-100 which dissolved the lipid membrane without interfering with the fluorescence signal. The percentage of calcein release was calculated according to the following equation:

$$\%\text{Calcein leakage} = (\text{Ft}–\text{Fo})/(\text{Ff}–\text{Fo}) * 100 \quad (1)$$

where the percent of calcein leakage is the fraction of dye released (normalized membrane leakage), Ft is the measured fluorescence intensity at time t, and Fo and Ff are respectively the fluorescence intensities at times $t = 0$, and after final addition of Triton X-100, respectively. A dilution correction was applied on the fluorescence intensity after injection of the Triton X-100. Each experiment was repeated three times.

2.10. Isothermal titration calorimetry (ITC)

ITC experiments were performed on a TA Instrument nano ITC calorimeter. To avoid air bubbles, peptide and LUV solutions were degassed under vacuum before use. Titrations were performed by injecting aliquots of LUVs (10 mg/mL of lipid were used) into the calorimeter cell containing the peptide solution (peptide concentration 0.1 mM), with 5 min waiting between injections (20–50 injections of 5 μL). The experiments were performed at 25 or 60 °C. Data analysis was performed using the program NanoAnalyze provided by TA Instruments.

2.11. Differential scanning calorimetry (DSC)

Data was acquired on a high-sensitivity differential scanning calorimeter (Calorimetry Sciences Corporation). A scan rate of 1 °C/min was used and there was a delay of 10 min between sequential scans in a series that allows for thermal equilibration. Data analysis was performed with the fitting program CPCALC provided by CSC and plotted with Igor. The total lipid concentrations used were 1 mg/mL, considering full hydration of the phospholipid mixtures. At peptide concentrations corresponding to those at the higher peptide/lipid molar ratios studied (P/L 1:10), peptides exhibited no thermal events over the temperature range of 0–100 °C. A minimum of at least three to four heating and cooling scans were performed for each analysis depending whether or not the spectra were reproducible.

2.12. Plasmon waveguide resonance (PWR) spectroscopy

PWR spectra are produced by resonance excitation of conduction electron oscillations (plasmons) by light from a polarized CW laser (He–Ne; wavelength of 632.8 and 543.5 nm) incident on the back surface of a thin metal film (Ag) deposited on a glass prism and coated with a layer of SiO_2 (see ref. [15] for additional information). Experiments were performed on a beta PWR instrument from Proterion Corp. (Piscataway, NJ) that had a spectral resolution of 1 mdeg. The method used to prepare the lipid bilayers has been previously described [15]. The molecules (such as lipids and peptides) deposited onto the surface plasmon resonator change the resonance characteristics of the plasmon formation and can thereby be detected and characterized. PWR resonances can be obtained with light whose electric vector is either parallel (*s*-polarization) or perpendicular (*p*-polarization) to the plane of the resonator surface. For oriented molecules, such as the lipid bilayers information both about mass changes (such as in SPR) but also changes in the anisotropy (not obtained with SPR) of the system can be obtained. Data fitting (GraphPad Prism) through a hyperbolic saturation curve provides the dissociation constants. Graphical

analysis of the spectral shifts obtained with both polarizations was performed to determine the contributions of mass and structural changes for each spectrum [16].

2.13. Circular dichroism (CD) spectroscopy

CD spectra of the peptides were recorded with a Jobin-Yvon CD6-SPEX dichrograph linked to a PC microprocessor. The instrument outputs were calibrated with D(+)-10-camphorsulfonic acid. The spectra were scanned at 25 °C and 60 °C in a quartz optical cell with a 1 mm path length. Spectra were recorded between 185 and 260 nm with 0.5 nm step. Eight scans were accumulated and averaged after buffer (or LUV) spectra subtraction and baseline correction. The peptide concentration was varied from 20 to 120 μM in 10 mM phosphate buffer (pH 7.6) and in presence of DSPC and DSPG LUVs (1250 μM and P/L ratios from 1/100 to 1/10). CD measurements are reported as $\Delta\varepsilon$ (M^{-1} cm^{-1}). No detailed analysis on CD spectra components was performed since deconvolution methods are based on protein structural information and are not straightforwardly adapted to small peptides.

2.14. ATR-FTIR spectroscopy

ATR-FTIR spectra were recorded with a Nicolet 6700 FT-IR spectrometer (Nicolet Instrument, Madison, WI) equipped with a liquid nitrogen 190 cooled mercury–cadmium–telluride detector on a Germanium crystal thermostated at 30 °C. ATR spectroscopy is sensitive to orientation and therefore spectra were recorded with a parallel (*p*) or perpendicular (*s*) polarization of the incident light with respect of the ATR plate. [17] 800 scans were co-added at a resolution of 8 cm^{-1}. Lipid bilayers were formed by the fusion of SUVs onto the ATR germanium crystal. Briefly, 20 μL of 1.5 mg/mL SUV solution was deposited on the crystal containing the Teflon cell. After 10–15 min, the non-adsorbed lipids were rinsed several times with buffer, following addition of 20 μL of deuterated buffer (10 mM Tris–HCl, pH 7.6) before the polarized *s* and *p* ATR-FTIR spectra were recorded. Once the bilayer was formed, the peptides were added to allow a final concentration in the cell of 1 mM. Spectra were recorded over time for both *p* and *s* polarizations after rinsing the cell with buffer to remove unbound peptide.

The amide I frequencies were attributed as follows: 1615–1625 cm^{-1} and 1685–1695 cm^{-1} antiparallel beta sheet, 1630–1635 cm^{-1} parallel beta sheet, 1640–1650 cm^{-1} random coil, 1650–1662 cm^{-1} alpha helix, and 1662–1680 cm^{-1} beta turn.

3. Results and discussion

3.1. Selective KLA–Pen conjugate cytotoxicity in human cancer cells

To examine the cytotoxic properties of the KLA–Pen conjugate, a range of human cell lines was used. It consists of seven cancer cell lines originating from non-small cell lung carcinoma (A549, Epo40, Epo480), neuroblastoma (SK-N-SH), glioblastoma (U87, U251), and colon carcinoma (SW480); as well as three non-cancer cell models including an embryonic kidney cell line (HEK293), a keratinocyte cell line (HaCaT) and vascular endothelial primary cells (HUVEC). As shown in Fig. 1A and B, KLA peptide alone (10 μM) did not exert any significant cytotoxic effects against all tested cell lines ($p > 0.05$). When conjugated to the cell-penetrating peptide penetratin, KLA–Pen exhibits significant *in vitro* anticancer activity. The seven different cancer cell lines were sensitive to the conjugate KLA–Pen (10 μM), which decreased cell survival from 40% in U251 cells to almost 70% in A549 cells after a 6 h-treatment ($p < 0.01$; Fig. 1A). In addition, the two glioblastoma cell lines U87 and U251 displayed different levels of sensitivity (Fig. 1A), supporting the fact that KLA–Pen efficacy does not depend on the tissue of origin. Interestingly, KLA–Pen was even efficient in decreasing cell survival in lung cancer Epo40 and Epo480 cells (Fig. 1A), which are highly resistant to conventional chemotherapy, *i.e.* microtubule-targeted agents (epothilone B or paclitaxel) and cisplatin (personal data) [18].

Efficacy of the conjugate was time-dependent, since survival of the same cell line A549 was inhibited by 54 ± 5% and 69 ± 4% after a 2 h (data not shown) and 6 h-treatment (Fig. 1A) respectively, and reached 84 ± 5% of inhibition after a 24 h-treatment (Fig. 1B). As shown in Fig. 1C, cancer cells cannot recover from this challenge, since a 24 h-incubation with KLA–Pen followed by a 24 h drug free period did not change efficacy of the conjugate. Of note is that it is necessary to conjugate KLA to penetratin since the respective effects cannot be met with the mixture of these peptides, even after a 24 h-incubation with cells ($p > 0.05$, Fig. 1B).

Lastly, these cytotoxicity assays revealed a selectivity of the conjugate for cancer cells, since none of the three non-cancer cell types tested was affected by KLA–Pen treatment (10 μM), whatever duration treatment was ($p > 0.05$; Fig. 1A and B).

3.2. KLA–Pen conjugate potently triggers mitochondrial network disruption in cancer cells

To further investigate the anticancer activity of KLA–Pen, we generated various cellular models stably expressing mt-DsRed or stained with MitoTracker, and the mitochondrial network was analyzed by live fluorescence microscopy. As expected, in vehicle-treated lung cancer A549 cells, mitochondria form elongated tubular and branched filaments (Fig. 2, control). Mitochondrial organization remained unchanged in A549 cells treated with KLA or penetratin alone (10 μM), for 10 min and 1 h (Fig. 2, left and right panels respectively) as well as for 6 h (Supplemental Fig. 1). In contrast, 10 μM of KLA–Pen conjugate highly disrupted the mitochondrial network organization. The entire A549 cell population displayed clusters of mitochondria after short time treatments (Fig. 2). We then confirmed the early impact of KLA–Pen on the mitochondrial architecture in other cancer cell types, since the network also changes from tubular to spherical in glioblastoma U87, neuroblastoma SK-N-SH and colon carcinoma SW480 cells (Fig. 3A and data not shown). Thus, while KLA and penetratin peptides alone are ineffective, their conjugation potently affects the mitochondrial organization. Mitochondria form a highly dynamic network that undergoes constant fusion and fission events, leading to changes in their overall morphology. These dynamics are essential for maintaining proper physiological functions and survival of cells [19]. Whereas most studies have focused on proteins involved in mitochondrial dynamics, growing pieces of evidence show that changes in membrane lipids also actively play roles in apoptosis induction by modulating the mitochondrial fission/fusion balance [20]. In that context, our data suggest a direct link between the cytotoxicity observed with the KLA–Pen conjugate and the organelle's excessive fusion. Moreover, in agreement with the cytotoxicity assays, our results show that KLA–Pen selectively acts on cancer cells, since the mitochondrial architecture was not altered in non-cancer HUVEC and HaCaT cells (Fig. 3B). One of the key differences between malignant and healthy mitochondria may be the high mitochondrial membrane potential ($\Delta\psi m$) [21]. Even slight gains in $\Delta\psi m$ have been proposed to confer to cationic agents a greater targeting of mitochondrial membranes and, consequently, better membrane permeabilization and cell death induction in cancer cells [22]. To further provide insight into the interaction of KLA with mitochondrial membrane lipids, a biophysical approach has been chosen (3.3 below).

3.3. Mode of interaction of KLA and KLA–Pen peptides with lipids

To mimic both the eukaryotic cell and the mitochondrial membrane lipid, model systems composed of zwitterionic phosphatidylcholine (PC) and anionic phosphatidylglycerol (PG) were employed, respectively. One should note that while the outer leaflet of a healthy eukaryotic cell is mainly composed of PC, in the case of cancer cells they become more anionic. As for the mitochondrial membranes, anionic lipids

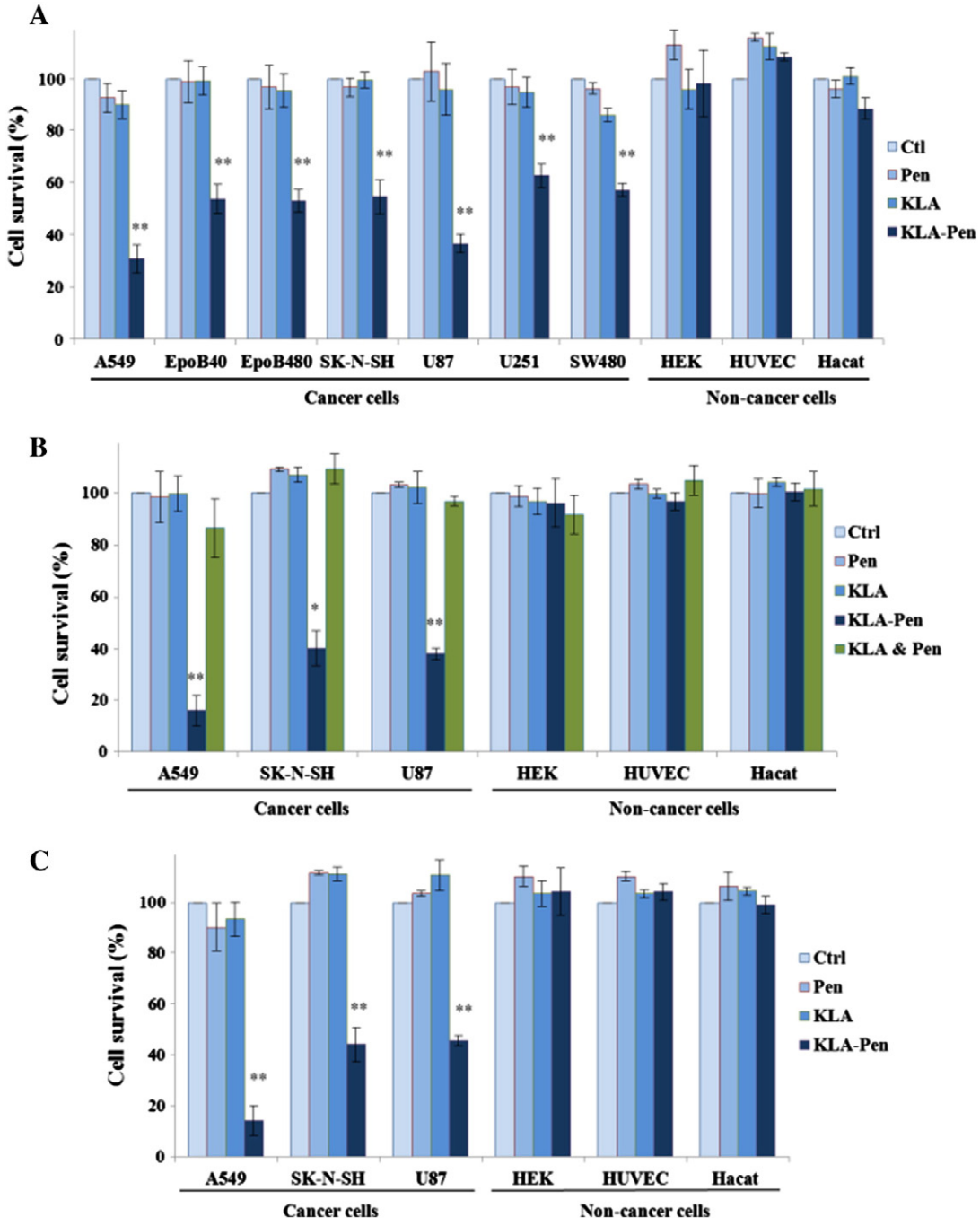

Fig. 1. Selective cytotoxic properties of Pen–KLA in cancer cells *versus* non-cancer cells. Growth inhibition assay performed on a panel of 10 human cell lines using MTT after (A) 6 h incubation or (B) 24 h incubation with vehicle (Ctrl), 10 μM penetratin (Pen), 10 μM KLA, 10 μM of the conjugate (KLA–Pen) or a mixture of 10 μM KLA and 10 μM penetratin (KLA & Pen). (C) Same experiments were performed after a 24 h treatment followed a 24 h wash-out period. Seven cancer cell lines were first used, including non-small cell lung carcinoma sensitive (A549) or highly resistant to conventional chemotherapy agents (EpoB40 and EpoB480), neuroblastoma (SK-N-SH), glioblastoma (U87, U251), and colon carcinoma (SW480) cells. Then, three non-cancer cell models including an embryonic kidney cell line (HEK293), a keratinocyte cell line (HaCaT) and vascular endothelial primary cells (HUVEC) were used. Statistical analysis was performed using Student's *t* test (*$p < 0.05$; **$p < 0.01$).

count for about 20% of the membrane. While those are rather simplistic models and do not fairly reflect the lipid composition of the cellular membrane, they can provide some first clues about the mechanism of action and selectivity of these peptides.

3.3.1. Peptide effect on liposome size, distribution and membrane integrity

The turbidity of samples and the size distribution of the liposomes following peptide addition provide information about eventual liposome aggregation and precipitation. None of the peptides changed the turbidity of zwitterionic lipids (DSPC) (data not shown). At 25 °C, all the peptides strongly increased the turbidity of anionic lipids (DSPG), which increased with the P/L ratio. At 65 °C, KLA did not change the turbidity of liposomes while penetratin and KLA–Pen increased slightly the turbidity, however at high P/L ratio (1/10) (Fig. 2 in SI).

DLS experiments were performed with DSPC and DSPG from 25 to 65 °C (every 5 °C) to scan both below and above the Tm (50–52 °C) (Fig. 3 in SI). The size and distribution of DSPC alone changed with the temperature, the objects being large and polydisperse below 50 °C

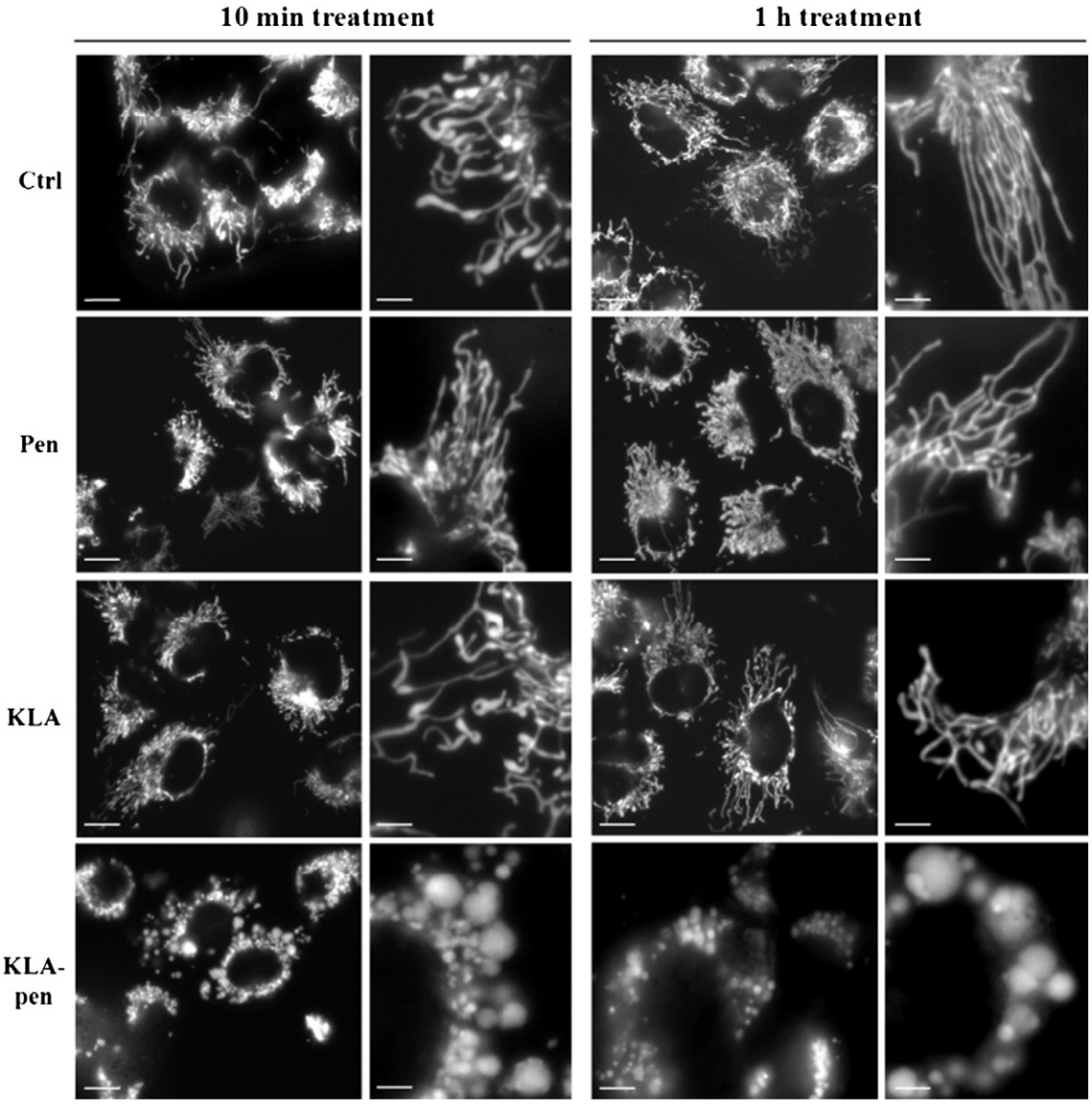

Fig. 2. Intense anti-mitochondrial effects of Pen–KLA in lung cancer cells. Representative photographs of lung cancer A549 cells stably expressing mtDsRed, incubated for 10 min (left panel) and 1 h (right panel) with 10 μM penetratin, KLA or KLA–Pen conjugate. Photographs were taken with the 40× objective of a Leica DM-IRBE microscope (scale bars for general views: 10 μm). Amplified views show the mitochondrial network of an individual cell in more details (scale bars for magnifications: 3 μm). At least three individual experiments were done.

and monodisperse above 50 °C (~100 nm) (Fig. 3A in SI). Above the Tm, DSPC liposomes are slightly larger (~120–140 nm) in the presence of the KLA–Pen conjugate, KLA or penetratin. This increase in the liposome size could arise from peptide interaction, although this does not seem to be the case as other experiments described below suggest no peptide interaction with zwitterionic lipids. One other possibility is that TFA present as counterion in the peptides interacts with the liposomes and leads to their swelling. At this point we have no other explanation for this observation. In the case of DSPG, liposomes have a homogeneous size, of around 100 nm, both below and above the Tm (Fig. 3B in SI). The addition of penetratin slightly increased the size of liposomes to about 115 nm below the Tm and the size decreased to about 100 above Tm. The increase in membrane fluidity at higher temperature allows better peptide penetration decreasing liposome size. In the case of KLA and KLA–Pen, the scenario is different, below Tm the peptides lead to heterogeneous objects and around Tm values and above both peptides lead to single objects of around 100 nm. This suggests changes in liposome aggregation and P/L interaction with temperature and will be further discussed below.

Calcein leakage experiments were performed to test the effect of the peptides on the membrane integrity, as some membrane amphipathic peptides induce pore formation. The experiments were performed with DOPC and DOPG, since the lipid must be in the fluid state (which is the case here at RT) so that there are no inherent membrane defaults and subsequent calcein leakage. Penetratin does not induce membrane leakage, while both KLA and KLA–Pen at low concentrations (P/L 1/100) induce leakage in liposomes made of DOPG (KLA to a greater extent that KLA–Pen), but not in liposomes made of DOPC (Fig. 4 in SI). Different types of pores have been proposed, to explain the action of antimicrobial and amphipathic peptides, that are composed by peptide alone (laying perpendicular to the membrane; barrel stave model), or a mixture of peptide and lipid where the peptide is oriented perpendicular (toroidal model) or is not oriented at all and works more like a detergent (carpet model) [23]. The following experiments shed some light on these aspects.

3.3.2. Thermodynamics of the P/L interaction

The affinity of the peptides to lipid model systems was investigated by ITC using both zwitterionic (DSPC) and anionic (DSPG) lipids with

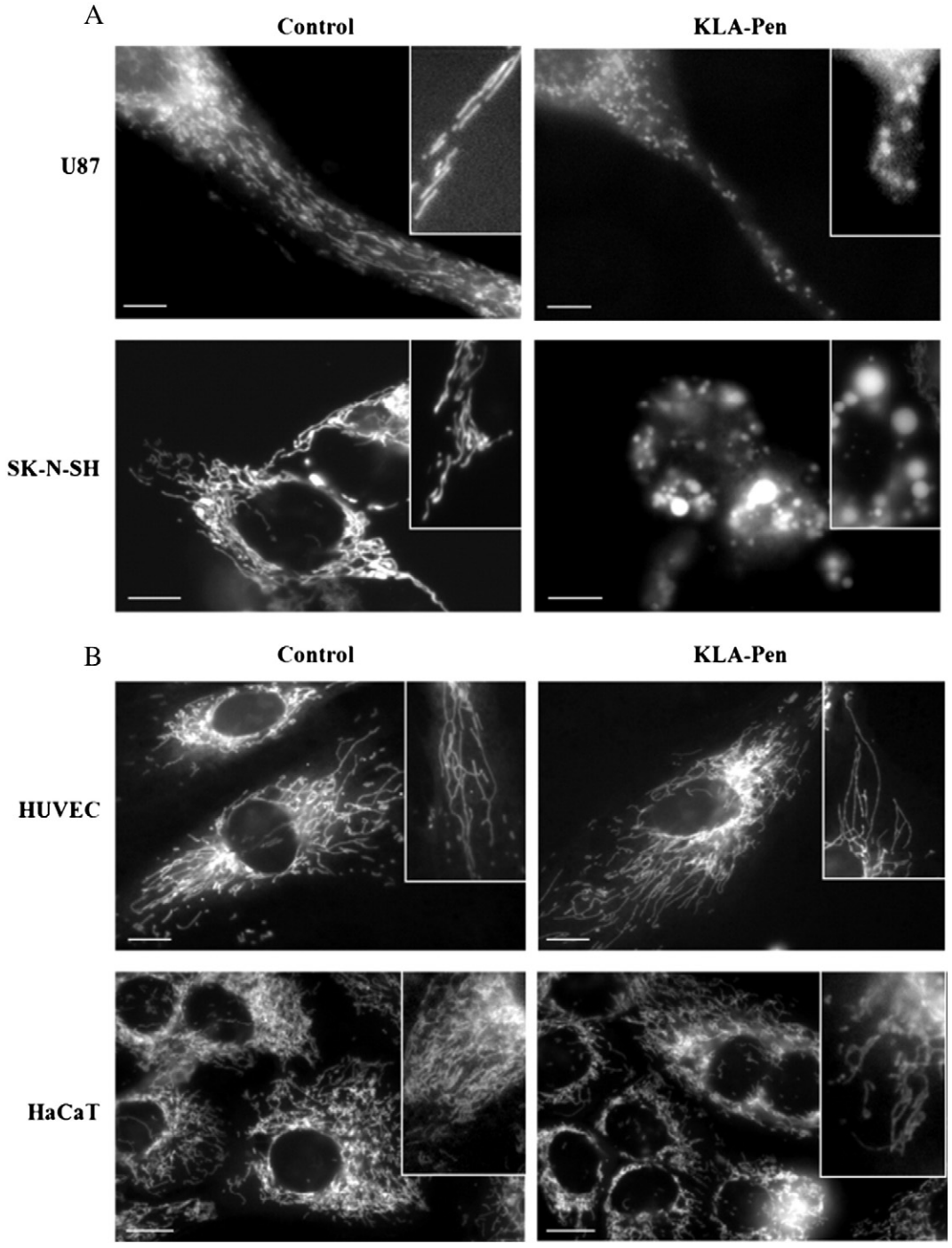

Fig. 3. Selective anti-mitochondrial effects of Pen–KLA in cancer *versus* non-cancer cells. (A) Representative photographs of glioblastoma U87 and neuroblastoma SK-N-SH cells stably expressing mtDsRed, incubated for 1 h with vehicule (control) or 10 μM of KLA–Pen conjugate (scale bars 5 μm). (B) Same experimental conditions with non-cancer HUVECs and HaCaT cells stained with MitoTracker Red (scale bars 10 μm). Photographs were taken with the 40× objective of a Leica DM-IRBE microscope. 2-times amplified views show the mitochondrial network of an individual cell in more details. At least three individual experiments were done.

experiments performed both below and above the Tm. For DSPC, heat exchanges observed upon incremental lipid addition to all the peptides were small and did not follow typical binding isotherms, the interaction being weak and/or associated with other processes (data not shown). The nature of KLA binding to DSPG changed with temperature, being exothermic below Tm and endothermic above, (Table 1, Fig. 4). At 25 °C and at high lipid concentration, precipitation may have occurred, as indicated by the small positive heats [24]. As far as we know, this is the first example shown in the literature where the sign of enthalpy of the reaction reversed under the same experimental conditions aside from the temperature. Below Tm, the interactions of the amphipathic KLA are both enthalpy and entropy favorable, reflecting good hydrogen bonding with the anionic DSPG and favorable hydrophobic interactions. The hydrophobic face of the peptide could be associated with other peptide molecules in a way to protect the hydrophobic face from unfavorable solvent interactions (as discussed below, CD results strengthen this hypothesis). KLA self-association has been previously reported [25]. Each peptide oligomer could interact with many liposomes explaining the changes in object size and turbidity induced by KLA in DSPG at temperatures below Tm. Above the Tm, P/L interactions

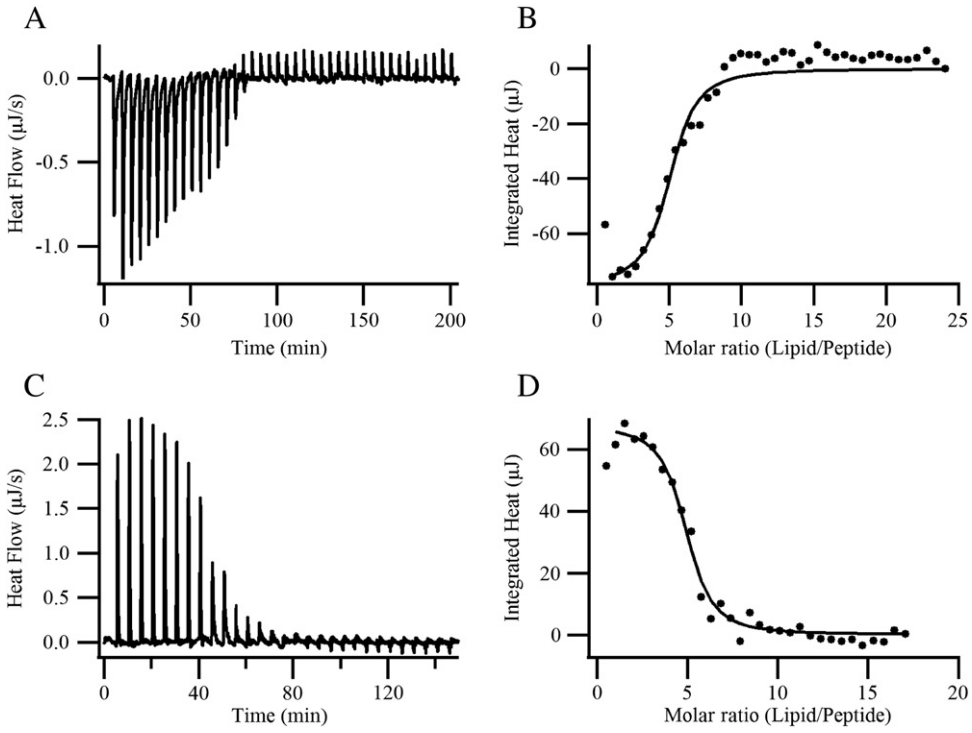

Fig. 4. Thermodynamics of P/L interaction. Titration of DSPG into KLA. (A and C) Calorimetric trace obtained at 25 °C and 60 °C, respectively, by titration of DSPG (10.4 mM) into a solution of KLA (100 μM). Each peak corresponds to the injection of 5 μL of DSPG into the calorimeter cell. (B and D) Heats of reaction (integrated from the calorimetric trace) plotted as a function of the lipid/peptide ratio. The solid line is the best fit to the experimental data with the parameters presented in Table 1.

become enthalpy unfavorable and entropy favorable, meaning the binding is mostly driven by hydrophobic interactions. With the increase in temperature, the lipid becomes more fluid, which should promote further insertion of KLA into the membrane and may disrupt hydrophobic peptide/peptide interactions that are now occurring between the peptide and the lipid. Such process would explain the decrease in liposome aggregation and particle size. These changes in KLA/DSPG interactions as a function of temperature are supported by other data (see below). Penetratin and KLA–Pen interactions with DSPG lead to exothermic reactions both below and above Tm and to K_D values in the same range (Table 1). The stoichiometry (n) that reflects the average number of lipid molecules bound per peptide molecules is very close to the number of charged residues in the peptide that is exactly 7 in the case of penetratin and 6 for KLA (Table 1). The experiments were then performed at different temperatures in order to determine the variation in heat capacity of the reaction (ΔCp) (data in SI, Fig. 5). This parameter can provide information about the nature of the predominant forces between the peptide and the lipids. A positive ΔCp is characteristic of electrostatic interactions that are mostly enthalpy driven while a negative value indicates a predominance of hydrophobic interactions [26]. A positive value was found for the interaction of penetratin with DSPG (3 J/mol) indicating that electrostatic interactions, associated with favorable enthalpy change, predominate. For KLA and KLA–Pen it was not possible to determine the value of the ΔCp because at several temperatures (from 40 to 60 °C) the isotherm was complex with both negative and positive titration peaks. It seems that for these two peptides the variation in temperature greatly affects the nature of the P/L interactions.

Table 1
Thermodynamic parameters of peptides binding to DSPG LUVs determined by ITC at 25 and 60 °C.

Peptides	Temperature (°C)	K_D (μM)	ΔH (KJ/mol)	N
KLA	25	18	−1.5	5
	60	8	1.3	5
Penetratin	25	12	−0.5	7
	60	21	−0.4	7
KLA–Pen	25	14	−1.9	11
	60	16	−1.8	11

DSC was performed with zwitterionic (DSPC and DMPC) and anionic (DSPG and DMPG) lipids to evaluate the effect of the peptides on the lipid phase transition. In all cases, addition of KLA has little influence on ΔH, but strongly affects Tm, which increases with peptide addition (Tables 1 and 2 in SI). This increase in Tm suggests that KLA stabilizes the gel phase state of the membrane. The effect of penetratin on the zwitterionic lipid phase transition is quite similar to that of KLA. With the anionic lipids, penetratin leads to a decrease (about 60%) in the enthalpy of the transition and an increase in Tm (about 1.5 °C) without much effect on the cooperativity of the transition (Tables 3 and 4 in SI). The effect of the KLA–Pen conjugate on the zwitterionic lipid phase transition is similar to that observed with KLA and penetratin. Whereas with anionic lipids, an increase in the Tm with a large decrease in the enthalpy of the transition (~60% decrease), were measured as for penetratin alone (Tables 5 and 6 in SI).

The increase in temperature, cooperativity and enthalpy of the transition in the case of zwitterionic lipids in the presence of all the peptides might be related to the changes in the ionic strength of the medium coming from the addition of the cationic peptides and their trifluoroacetate counterions. Changes in pH and ionic composition of the medium have been shown to alter the lipid phase transition properties [27].

3.3.3. Peptide secondary structure and orientation when interacting with the membrane

In buffer and with zwitterionic lipids (DSPC) the peptides were all non-structured (random coil) as observed on CD spectra (Fig. 6 in SI). In the presence of anionic lipids (DSPG), the peptides become structured in α-helix. The $[\theta]_{222}/[\theta]_{208}$ ratio was used to obtain information on the presence of coiled-coil helices: values greater than 1 indicate the presence of coiled coils due to peptide self-association values below 1 are characteristic of non-interacting helices [28]. The capacity of the peptides to self-associate is affected by the temperature, and so

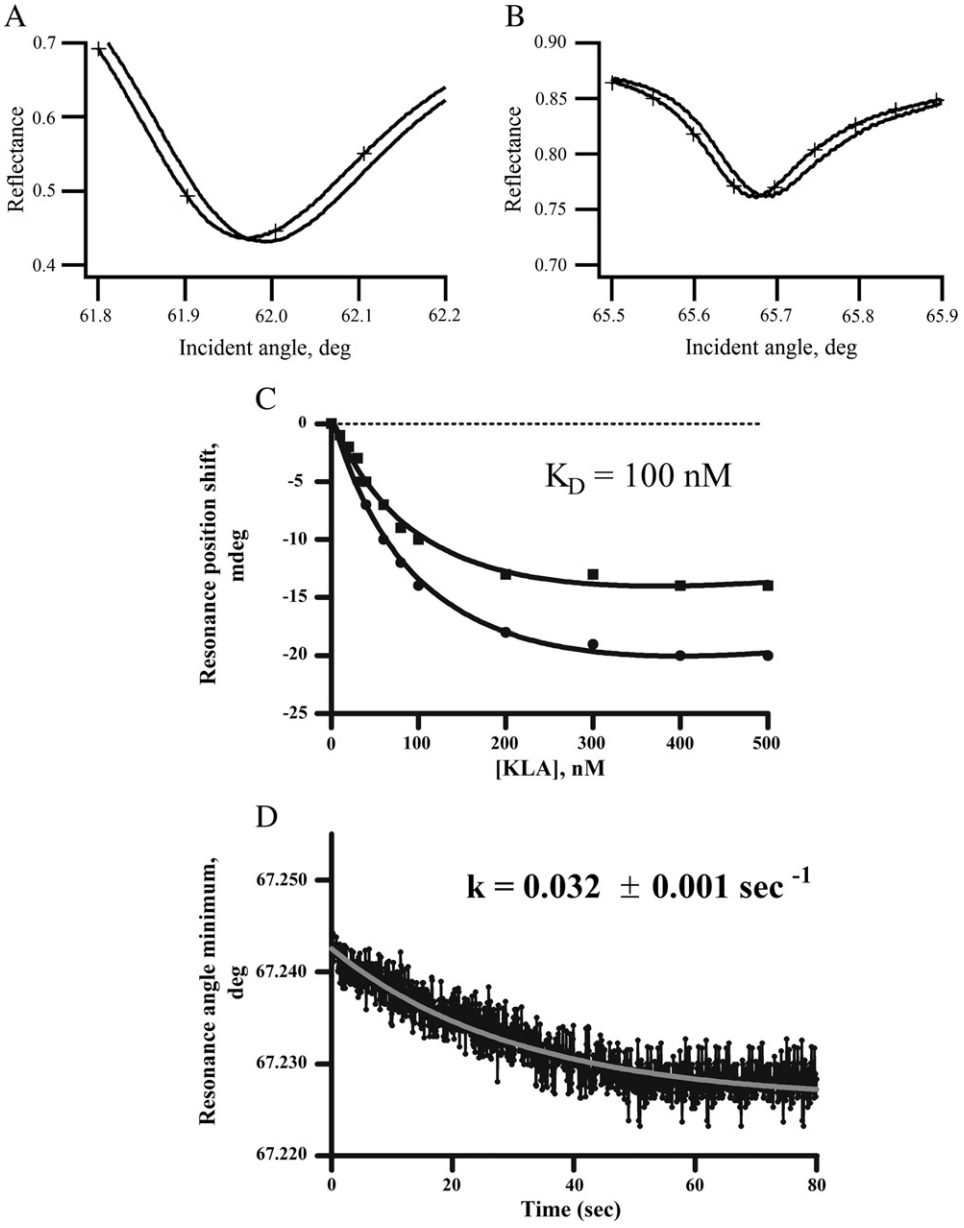

Fig. 5. KLA interaction with a DMPG bilayer investigated by PWR. Panels A and B correspond to the PWR spectra of a lipid bilayer alone (solid line) and upon addition of saturating amounts of KLA (+). The resonance position shifts obtained upon incremental addition of KLA to the membrane with the *p*- (●) and *s*-pol (■) are presented in panel C, together with the hyperbolic binding curve (K_D values are presented in Table 6). Panel D corresponds to the kinetic measurements obtained for the p-pol light upon addition of 0.1 μM of KLA to the DMPG bilayer (rate constants are provided in Table 3).

the phase of the lipid. In the case of KLA, at 25 °C the $[\theta]_{222}/[\theta]_{208}$ ratio is higher than 1 (associated helices) while at 60 °C the ratio is now lower than 1, meaning that the helices are isolated. For penetratin and the conjugated KLA–Pen, the situation is quite similar to KLA with associated helices at temperatures below the Tm and isolated helices above it.

Polarized ATR-FTIR spectroscopy provided information on the orientation of the peptide relative to the lipid membrane as well as effects of the peptide on the lipid organization [29]. The experiments were performed with DMPC and DMPC/DMPG (8/2 mol/mol) so that the lipids are fluid at room temperature. No pure anionic lipid was used, as in other experiments because from our own experience membranes cannot be formed by SUV fusion containing pure PG (the maximum quantity of PG that can be used is 20–30%). In the case of DMPC, for all peptides investigated, no typical peptide secondary structure bands were observed (amide I and II bands), even at high concentration of peptide (1 mM). Additionally, no change was induced in the lipid typical bands, further suggesting that the peptide did not interact with zwitterionic lipids. But, in the presence of DMPG (20% relative to DMPC), all the cationic peptides remained attached even after washing the cell with buffer and incorporated into the membrane with a P/L around 1/150. The decomposition of the amide I band in single component characteristic of each secondary structure (Fig. 7 in SI) allowed the determination of the peptides secondary structures in the presence of this lipid (Table 2). The three peptides display quite comparable secondary structure with a predominance of random coil (40%) and α-helix (30%) following by some antiparallel β-sheet (20%) and some β-turn and/or signal corresponding to TFA (10%), (this counterion absorbs in the same region as the β-turn, around 1670 cm^{-1}). The orientation of the α-helix in the peptide was estimated from the dichroic ratio (obtained from the *p* and *s* polarized spectra). With a value close to 1 for penetratin, the α-helical component of the Pen is lying flat on the lipid bilayer. In the case of both KLA and KLA–Pen, the dichroic ratio around 1.6–1.7 suggests a tilted orientation of the helix main axis with an angle around 55° with the respect to the crystal normal (Table 2). This tilted

Table 2
Secondary structure of the peptides in presence of DMPC/DMPG (8/2 mol/mol) as determined by ATR-FTIR.

Secondary structure composition (%)	KLA (P/L ≈ 1/150)	Penetratin (P/L ≈ 1/135)	KLA–Pen (P/L ≈ 1/155)
Antiparallel β-sheet	18	21	16
Random	43	35	39
α-Helix	34 (R_{ATR} ≈ 1.6)	29 (R_{ATR} ≈ 1.0)	35 (R_{ATR} ≈ 1.7)
β-Turn[a]	5	15	10

[a] The trifluoroacetate (TFA) counterions for the peptides strongly contribute also to this region.

orientation for the peptide may be at the origin of the calcein leakage induced by both KLA and KLA–Pen with the formation of pores in the membrane (see above). The preference for this particular peptide orientation suggested a pore of the type barrel stave or toroidal rather than a mechanism by detergent disruption. Regarding peptide effects on lipid organization, none of the peptides significantly affected the Ap/As ratios of the symmetric stretching of CH_2, meaning that overall they did not greatly affect the acyl chain orientation. However, the absolute values of all the methylene wavenumbers increased for all the peptides (variations ranged from 3 to 7 cm^{-1}). Such increase indicates that the peptides insert deeply enough in the fatty acid chain region of the membrane and modify the lipid organization inducing an increase of disorder.

3.3.4. Affinity and kinetics of peptide interaction with lipids and subsequent lipid reorganization

Plasmon waveguide resonance (PWR) was used to determine the affinity and kinetics of peptide interaction with planar lipid bilayers composed of DMPC and DMPG in the fluid phase. The addition of KLA, penetratin or KLA–Pen to a DMPC lipid bilayer (for concentrations up to 100 μM of peptide in the cell) did not produce significant shifts in the resonance angle position (data not shown), suggesting that none of these peptides interacts with this zwitterionic lipid. The results correlate well with ITC experiments that also indicate a lack of interaction with DMPC (data not shown). In the case of DMPG, KLA leads to a decrease in the resonance angle position for both polarizations (Fig. 5, Table 5 in SI), which corresponds to a decrease in mass in the system. Such mass loss can be due to a partial solubilization of the membrane and/or pore formation, which correlates well with calcein leakage studies. The spectral shifts induced by the peptide were anisotropic (with shifts in the *p*-polarization being higher than in *s*-polarization), indicating that the peptide induces larger changes in mass and structure perpendicularly to the membrane. Such results corroborate well with ATR-FTIR studies suggesting an oblique orientation of the peptide helix within the bilayer. A graphical analysis was performed to determine the structural and mass contributions to the spectral change (Table 4 in SI). A major mass contribution was observed with a value of 85% for KLA and an apparent dissociation constant for P/L interaction was determined to be 0.1 μM from the resonance minimum position changes as a function of peptide concentrations, (Fig. 5, Table 3). Additionally, the kinetics of the interaction with the bilayer was followed by measuring the resonance minimum position as a function of time upon addition of 0.1 μM of KLA to the DMPG membrane. A rate constant of 0.032 s^{-1} was determined for this interaction (Table 3). As previously reported for penetratin, its interaction with DMPG lead to an apparent K_D value of 0.3 μM with and a kinetic constant of 0.090 s^{-1}, which is slightly faster but in the same magnitude as that observed for KLA (Table 3) [30]. For KLA–Pen, like KLA the spectral changes were dominated by mass changes, (Table 4 in SI), (in this case decreases in mass) mainly attributed to lipid reorganization (as explained above). An apparent K_D value of 0.1 μM was observed and a kinetic constant of 0.045 s^{-1} (Table 3).

Table 3
Affinity and kinetics of the interaction of the peptides with DMPG lipid bilayer determined by PWR.

Peptides	K_D (μM)	k (s^{-1})
KLA	0.1 ± 0.003	0.032 ± 0.002
Penetratin	0.3 ± 0.002	0.090 ± 0.004
KLA–Pen	0.1 ± 0.002	0.045 ± 0.005

The constants result from 3 independent experiments.

4. Conclusions

CPPs have become important tools for the cellular delivery of a wide range of molecules including pharmaceuticals. The proapoptotic peptide KLA cannot efficiently permeate across eukaryotic plasma membranes and consequently exhibits low mammalian cell cytotoxicity. We chose here to conjugate it to the cell penetrating peptide penetratin to facilitate cellular uptake. We first demonstrated that the conjugated KLA–Pen peptide has cytotoxic properties against a panel of seven human cancer cell lines of various tissue origins, including cells resistant to some conventional chemotherapy agents. Interestingly, KLA–Pen did not affect, at the same concentration, the different human non-cancer cell lines or primary cultures, highlighting a selective anti-cancer activity *in vitro* for this conjugated peptide. In an attempt to understand some of the reasons behind KLA–Pen selectivity for tumor cells and deleterious action on mitochondrial membranes, a biophysical approach was used with simple lipid membrane models mimicking normal and tumor eukaryotic cell membranes, as well as mitochondrial membranes. While differences in terms of the proteoglycan composition between tumor and non-tumor cell lines have been reported in the literature which may affect the endocytic pathway taken by the conjugate in the types of cells, herein we have only focused on the differences in lipid composition of the two cell types. The results show that KLA–Pen interacts and affects the organization of an anionic lipid membrane model (representative model of a cancer cell membrane) while it does not bind to a zwitterionic membrane (non-cancer cell membrane). Indeed with anionic lipids the conjugate leads to liposome aggregation and leakage, has a disordering effect on lipid organization and inserts in membrane with a tilted orientation relative to the membrane. The KLA–Pen conjugate may exert its deleterious action on charged membranes by the formation of pores where the conjugate orients obliquely in the membrane and establishes important hydrophobic interactions. Such selective interaction with anionic membranes supports the selectivity observed in cancer cells. Membranes of cancer cells have also been reported to be more fluid than those of "normal" cells, which may further facilitate peptide penetration and perturbation [31]. Very preliminary results obtained with propidium iodide showed that KLA–PEN could increase more efficiently the fluorescent probe uptake in cancer cells as compared with non-cancer cells (personal data). Nevertheless, a complete examination of phosphatidylserine composition and efflux/influx through plasma membrane of cancer and non-cancer cells will be necessary to clarify the mechanism behind the selective targeting of KLA–Pen conjugate.

Cancer cell death induction upon chemotherapy drug treatment has been generally linked to mitochondrial fragmentation into small individual organelles [32]. In contrast, the present study suggests that the KLA–Pen conjugate induces an excessive fusion of mitochondria in cancer cells, resulting in huge damages in the mitochondrial architecture and in the inhibition of their metabolic activity [33]. Once inside the cell, KLA is rather active towards the mitochondria which, among other properties, are characterized by the marked anionic character

in the lipid membrane composition (presence of cardiolipin). The biophysical studies with anionic membranes (*i.e.* representative of mitochondria anionic character) demonstrate the strong impact of this peptide on the supramolecular organization of lipids with strong liposome aggregation, leakage (formation of pores) and lipid disordering effects. Interestingly, these processes correlate with both the effects we observed on mitochondrial network architecture, and the well-known KLA-mediated release of pro-apoptotic factors from mitochondria that ultimately results in cell death.

Overall, the biophysical studies performed allowed us to conclude that, in addition to electrostatic interactions that might be at the origin of the observed selectivity, interactions of KLA and the conjugate peptide with lipids is very much influenced by the fluidity state of the membrane (a process dependent on both membrane composition and temperature). Such parameters (electrostatics, membrane fluidity and temperature) seem to also influence the oligomerization state of the peptide, which strongly affects the peptide mode of action. Here very simple lipid model systems were used that are quite far from the real composition of a cell or mitochondria membrane. Nonetheless these studies provide us some clues on the mechanism of action of these peptides. Future studies with models whose composition resembles more in the cell membrane and mitochondria are considered. The mitochondria have recently gained in interest since they are now considered as potential druggable targets for successful rational drug design and therapy. The key point is that strategies that directly engage mitochondria could bypass resistance to apoptosis that normally arises as a consequence of accumulation of mutations in apoptosis signaling intermediates upstream of mitochondria in a variety of cancers [34]. Combining mitochondria-targeted peptides with low doses of conventional chemotherapy may thus be a powerful strategy to synergistically induce cancer cell death while reducing acquired resistance and side effects.

Acknowledgements

The authors would like to thank Susan B. Horwitz (Albert Einstein College of Medicine, New York, USA) which kindly provided the A549.EpoB40 and EpoB480 cells. The research was partially funded by “La ligue contre le cancer”. This work has also been carried out thanks to the support of INCa-DGOS-Inserm 6038 (SIRIC label), and A*MIDEX project (no. ANR-11-IDEX-0001-02) funded by the “Investissements d'Avenir” French Government program, managed by the ANR.

Appendix A. Supplementary data

Supplementary data to this article can be found online at http://dx.doi.org/10.1016/j.bbamem.2014.04.025.

References

[1] C. Bechara, S. Sagan, Cell-penetrating peptides: 20 years later, where do we stand? *FEBS letters*, 2013.;
(b) B. Gupta, T.S. Levchenko, V.P. Torchilin, Intracellular delivery of large molecules and small particles by cell-penetrating proteins and peptides, Adv. Drug Deliv. Rev. 57 (4) (2005) 637–651;
(c) G.P. Dietz, M. Bahr, Delivery of bioactive molecules into the cell: the Trojan horse approach, Mol. Cell. Neurosci. 27 (2) (2004) 85–131;
(d) M. Mae, U. Langel, Cell-penetrating peptides as vectors for peptide, protein and oligonucleotide delivery, Curr. Opin. Pharmacol. 6 (5) (2006) 509–514;
(e) T. Lehto, K. Kurrikoff, U. Langel, Cell-penetrating peptides for the delivery of nucleic acids, Expert Opin. Drug Deliv. 9 (7) (2012) 823–836;
(f) P. Jarver, K. Langel, S. El-Andaloussi, U. Langel, Applications of cell-penetrating peptides in regulation of gene expression, Biochem. Soc. Trans. 35 (Pt 4) (2007) 770–774.
[2] D. Derossi, A.H. Joliot, G. Chassaing, A. Prochiantz, The third helix of the Antennapedia homeodomain translocates through biological membranes, J. Biol. Chem. 269 (14) (1994) 10444–10450.
[3] (a) T. Letoha, S. Gaal, C. Somlai, A. Czajlik, A. Perczel, B. Penke, Membrane translocation of penetratin and its derivatives in different cell lines, J. Mol. Recognit. 16 (5) (2003) 272–279;
(b) E. Dupont, A. Prochiantz, A. Joliot, Penetratin story: an overview, Methods Mol. Biol. 683 (2011) 21–29;
(c) I.D. Alves, C.Y. Jiao, S. Aubry, B. Aussedat, F. Burlina, G. Chassaing, S. Sagan, Cell biology meets biophysics to unveil the different mechanisms of penetratin internalization in cells, Biochim. Biophys. Acta 1798 (12) (2010) 2231–2239.
[4] M.M. Javadpour, M.M. Juban, W.C. Lo, S.M. Bishop, J.B. Alberty, S.M. Cowell, C.L. Becker, M.L. McLaughlin, De novo antimicrobial peptides with low mammalian cell toxicity, J. Med. Chem. 39 (16) (1996) 3107–3113.
[5] (a) V.R. Fantin, M.J. Berardi, H. Babbe, M.V. Michelman, C.M. Manning, P. Leder, A bifunctional targeted peptide that blocks HER-2 tyrosine kinase and disables mitochondrial function in HER-2-positive carcinoma cells, Cancer Res. 65 (15) (2005) 6891–6900;
(b) R. Smolarczyk, T. Cichon, K. Graja, J. Hucz, A. Sochanik, S. Szala, Antitumor effect of RGD-4C-GG-D(KLAKLAK)2 peptide in mouse B16(F10) melanoma model, Acta Biochim. Pol. 53 (4) (2006) 801–805.
[6] (a) S. Fulda, L. Galluzzi, G. Kroemer, Targeting mitochondria for cancer therapy, Nat. Rev. Drug Discov. 9 (6) (2010) 447–464;
(b) M. Cuperlovic-Culf, A.S. Culf, M. Touaibia, N. Lefort, Targeting the latest hallmark of cancer: another attempt at 'magic bullet' drugs targeting cancers' metabolic phenotype, Future Oncol. 8 (10) (2012) 1315–1330.
[7] H.M. Ellerby, W. Arap, L.M. Ellerby, R. Kain, R. Andrusiak, G.D. Rio, S. Krajewski, C.R. Lombardo, R. Rao, E. Ruoslahti, D.E. Bredesen, R. Pasqualini, Anti-cancer activity of targeted pro-apoptotic peptides, Nat. Med. 5 (9) (1999) 1032–1038.
[8] B. Law, L. Quinti, Y. Choi, R. Weissleder, C.H. Tung, A mitochondrial targeted fusion peptide exhibits remarkable cytotoxicity, Mol. Cancer Ther. 5 (8) (2006) 1944–1949.
[9] A.J. Marks, M.S. Cooper, R.J. Anderson, K.H. Orchard, G. Hale, J.M. North, K. Ganeshaguru, A.J. Steele, A.B. Mehta, M.W. Lowdell, R.G. Wickremasinghe, Selective apoptotic killing of malignant hemopoietic cells by antibody-targeted delivery of an amphipathic peptide, Cancer Res. 65 (6) (2005) 2373–2377.
[10] (a) J. Muller, J. Triebus, I. Kretzschmar, R. Volkmer, P. Boisguerin, The agony of choice: how to find a suitable CPP for cargo delivery, J. Pept. Sci. 18 (5) (2012) 293–301;
(b) M. Sioud, A. Mobergslien, Selective killing of cancer cells by peptide-targeted delivery of an anti-microbial peptide, Biochem. Pharmacol. 84 (9) (2012) 1123–1132.
[11] M. Zorko, U. Langel, Cell-penetrating peptides: mechanism and kinetics of cargo delivery, Adv. Drug Deliv. Rev. 57 (4) (2005) 529–545.
[12] (a) J. Connor, C. Bucana, I.J. Fidler, A.J. Schroit, Differentiation-dependent expression of phosphatidylserine in mammalian plasma membranes: quantitative assessment of outer-leaflet lipid by prothrombinase complex formation, Proc. Natl. Acad. Sci. U. S. A. 86 (9) (1989) 3184–3188;
(b) T. Utsugi, A.J. Schroit, J. Connor, C.D. Bucana, I.J. Fidler, Elevated expression of phosphatidylserine in the outer membrane leaflet of human tumor cells and recognition by activated human blood monocytes, Cancer Res. 51 (11) (1991) 3062–3066.
[13] (a) K. Matsuda, H. Maruyama, F. Guo, J. Kleeff, J. Itakura, Y. Matsumoto, A.D. Lander, M. Korc, Glypican-1 is overexpressed in human breast cancer and modulates the mitogenic effects of multiple heparin-binding growth factors in breast cancer cells, Cancer Res. 61 (14) (2001) 5562–5569;
(b) J.H. Lee, H. Park, H. Chung, S. Choi, Y. Kim, H. Yoo, T.Y. Kim, H.J. Hann, I. Seong, J. Kim, K.G. Kang, I.O. Han, E.S. Oh, Syndecan-2 regulates the migratory potential of melanoma cells, J. Biol. Chem. 284 (40) (2009) 27167–27175;
(c) R.D. Sanderson, Heparan sulfate proteoglycans in invasion and metastasis, Semin. Cell Dev. Biol. 12 (2) (2001) 89–98;
(d) I. Vlodavsky, O. Goldshmidt, E. Zcharia, R. Atzmon, Z. Rangini-Guatta, M. Elkin, T. Peretz, Y. Friedmann, Mammalian heparanase: involvement in cancer metastasis, angiogenesis and normal development, Semin. Cancer Biol. 12 (2) (2002) 121–129.
[14] G. Rouser, S. Fkeischer, A. Yamamoto, Two dimensional then layer chromatographic separation of polar lipids and determination of phospholipids by phosphorus analysis of spots, Lipids 5 (5) (1970) 494–496.
[15] Z. Salamon, H.A. Macleod, G. Tollin, Coupled plasmon-waveguide resonators: a new spectroscopic tool for probing proteolipid film structure and properties, Biophys. J. 73 (5) (1997) 2791–2797.
[16] Z. Salamon, G. Tollin, Graphical analysis of mass and anisotropy changes observed by plasmon-waveguide resonance spectroscopy can provide useful insights into membrane protein function, Biophys. J. 86 (4) (2004) 2508–2516.
[17] E. Goormaghtigh, V. Raussens, J.M. Ruysschaert, Attenuated total reflection infrared spectroscopy of proteins and lipids in biological membranes, Biochim. Biophys. Acta 1422 (2) (1999) 105–185.
[18] C.P. Yang, P. Verdier-Pinard, F. Wang, E. Lippaine-Horvath, L. He, D. Li, G. Hofle, I. Ojima, G.A. Orr, S.B. Horwitz, A highly epothilone B-resistant A549 cell line with mutations in tubulin that confer drug dependence, Mol. Cancer Ther. 4 (6) (2005) 987–995.
[19] D.F. Suen, K.L. Norris, R.J. Youle, Mitochondrial dynamics and apoptosis, Genes Dev. 22 (12) (2008) 1577–1590.
[20] H. Huang, M.A. Frohman, Visualizing mitochondrial lipids and fusion events in mammalian cells, Methods Cell Biol. 108 (2012) 131–145.
[21] M.A. Houston, L.H. Augenlicht, B.G. Heerdt, Stable differences in intrinsic mitochondrial membrane potential of tumor cell subpopulations reflect phenotypic heterogeneity, Int J Cell Biol 2011 (2011) 978583.
[22] J.E. Constance, C.S. Lim, Targeting malignant mitochondria with therapeutic peptides, Ther. Deliv. 3 (8) (2012) 961–979.
[23] (a) D.I. Chan, E.J. Prenner, H.J. Vogel, Tryptophan- and arginine-rich antimicrobial peptides: structures and mechanisms of action, Biochim. Biophys. Acta 1758 (9) (2006) 1184–1202;

(b) E.F. Haney, S. Nathoo, H.J. Vogel, E.J. Prenner, Induction of non-lamellar lipid phases by antimicrobial peptides: a potential link to mode of action, Chem. Phys. Lipids 163 (1) (2010) 82–93;
(c) K.A. Brogden, Antimicrobial peptides: pore formers or metabolic inhibitors in bacteria? Nat. Rev. Microbiol. 3 (3) (2005) 238–250.
[24] T. Wieprecht, O. Apostolov, M. Beyermann, J. Seelig, Membrane binding and pore formation of the antibacterial peptide PGLa: thermodynamic and mechanistic aspects, Biochemistry 39 (2) (2000) 442–452.
[25] M.M. Javadpour, M.D. Barkley, Self-assembly of designed antimicrobial peptides in solution and micelles, Biochemistry 36 (31) (1997) 9540–9549.
[26] (a) J. Seelig, Thermodynamics of lipid–peptide interactions, Biochim. Biophys. Acta 1666 (1–2) (2004) 40–50;
(b) B.M. Baker, K.P. Murphy, Prediction of binding energetics from structure using empirical parameterization, Methods Enzymol. 295 (1998) 294–315;
(c) M. Hoernke, C. Schwieger, A. Kerth, A. Blume, Binding of cationic pentapeptides with modified side chain lengths to negatively charged lipid membranes: Complex interplay of electrostatic and hydrophobic interactions, Biochim. Biophys. Acta 1818 (7) (2012) 1663–1672.
[27] (a) H. Trauble, H. Eibl, Electrostatic effects on lipid phase transitions: membrane structure and ionic environment, Proc. Natl. Acad. Sci. U. S. A. 71 (1) (1974) 214–219;
(b) S.S. Korreman, D. Posselt, Modification of anomalous swelling in multilamellar vesicles induced by alkali halide salts, Eur. Biophys. J. 30 (2) (2001) 121–128;
(c) D. Chapman, W.E. Peel, B. Kingston, T.H. Lilley, Lipid phase transitions in model biomembranes. The effect of ions on phosphatidylcholine bilayers. Biochim. Biophys. Acta 464 (2) (1977) 260–275;
(d) B.A. Cunningham, J.E. Shimotake, W. Tamura-Lis, T. Mastran, W.M. Kwok, J.W. Kauffman, L.J. Lis, The influence of ion species on phosphatidylcholine bilayer structure and packing, Chem. Phys. Lipids 39 (1–2) (1986) 135–143.
[28] (a) A.S. Ladokhin, M.E. Selsted, S.H. White, CD spectra of indolicidin antimicrobial peptides suggest turns, not polyproline helix, Biochemistry 38 (38) (1999) 12313–12319;
(b) S. Nagpal, V. Gupta, K.J. Kaur, D.M. Salunke, Structure-function analysis of tritrypticin, an antibacterial peptide of innate immune origin, J. Biol. Chem. 274 (33) (1999) 23296–23304.
[29] S. Castano, B. Desbat, Structure and orientation study of fusion peptide FP23 of gp41 from HIV-1 alone or inserted into various lipid membrane models (mono-, bi- and multibi-layers) by FT-IR spectroscopies and Brewster angle microscopy, Biochim. Biophys. Acta 1715 (2) (2005) 81–95.
[30] (a) I.D. Alves, C. Bechara, A. Walrant, Y. Zaltsman, C.Y. Jiao, S. Sagan, Relationships between membrane binding, affinity and cell internalization efficacy of a cell-penetrating peptide: penetratin as a case study, PLoS One 6 (9) (2011) e24096;
(b) I.D. Alves, I. Correia, C.Y. Jiao, E. Sachon, S. Sagan, S. Lavielle, G. Tollin, G. Chassaing, The interaction of cell-penetrating peptides with lipid model systems and subsequent lipid reorganization: thermodynamic and structural characterization, J. Pept. Sci. 15 (3) (2009) 200–209;
(c) I.D. Alves, N. Goasdoue, I. Correia, S. Aubry, C. Galanth, S. Sagan, S. Lavielle, G. Chassaing, Membrane interaction and perturbation mechanisms induced by two cationic cell penetrating peptides with distinct charge distribution, Biochim. Biophys. Acta 1780 (7–8) (2008) 948–959.
[31] M. Sok, M. Sentjurc, M. Schara, Membrane fluidity characteristics of human lung cancer, Cancer Lett. 139 (2) (1999) 215–220.
[32] (a) T. Landes, J.C. Martinou, Mitochondrial outer membrane permeabilization during apoptosis: the role of mitochondrial fission, Biochim. Biophys. Acta 1813 (4) (2011) 540–545;
(b) A. Savry, M. Carre, R. Berges, A. Rovini, I. Pobel, C. Chacon, D. Braguer, V. Bourgarel-Rey, Bcl-2-enhanced efficacy of microtubule-targeting chemotherapy through Bim overexpression: implications for cancer treatment, Neoplasia 15 (1) (2013) 49–60.
[33] V.V. Lemeshko, Potential-dependent membrane permeabilization and mitochondrial aggregation caused by anticancer polyarginine-KLA peptides, Arch. Biochem. Biophys. 493 (2) (2010) 213–220.
[34] S.J. Ralph, S. Rodriguez-Enriquez, J. Neuzil, E. Saavedra, R. Moreno-Sanchez, The causes of cancer revisited: "mitochondrial malignancy" and ROS-induced oncogenic transformation — why mitochondria are targets for cancer therapy, Mol. Asp. Med. 31 (2) (2010) 145–170